The various facets of random walk entropy[*]

Z. Burda, J. Duda

Marian Smoluchowski Institute of Physics, Jagellonian University, Reymonta 4,
30-059 Kraków, Poland

AND

J.M. Luck

Institut de Physique Théorique, CEA IPhT and CNRS URA 2306, CEA Saclay,
91191 Gif-sur-Yvette cedex, France

AND

B. Waclaw

SUPA, School of Physics and Astronomy, University of Edinburgh, Mayfield
Road, Edinburgh EH9 3JZ, UK

We review various features of the statistics of random paths on graphs. The relationship between path statistics and Quantum Mechanics (QM) leads to two canonical ways of defining random walk on a graph, which have different statistics and hence different entropies. Generic random walk (GRW) is in correspondence with the field-theoretical formalism, whereas maximal entropy random walk (MERW), introduced by us in a recent work, is motivated by the Feynman path-integral formulation of QM. GRW maximizes entropy locally (neighbors are chosen with equal probabilities), in contrast to MERW which does so globally (all paths of given length and endpoints are equally probable). The stationary distribution for MERW is given by the ground state of a quantum-mechanical problem where nodes whose degree is smaller than average act as repulsive impurities. We investigate static and dynamical properties GRW and MERW in a variety of examples in one and two dimensions. The most spectacular difference arises in the case of weakly diluted lattices, where a particle performing MERW gets eventually trapped in the largest nearly spherical region which is free of

---

[*] Based on a lecture presented by Z.B. at the 22nd Marian Smoluchowski Symposium on Statistical Physics (Zakopane, Poland, September 12–17, 2009).

impurities. We put forward a quantitative explanation of this localization effect in terms of a classical Lifshitz phenomenon.

1. Introduction

This paper presents a review of various facets of the statistics of random walks on graphs and other geometrical structures. Brownian motion has been proposed in the seminal works by Einstein [1] and Smoluchowski [2] as a microscopic theory for diffusive transport. Random walk (RW) models stem from a discretization of Brownian motion. The discretization procedure can be motivated either on theoretical grounds (it provides a cutoff regularizing the short-distance singularities which plague the continuous Brownian motion) or by practical considerations (it makes numerical simulations easier). There are many incarnations of RW, where either space or time is separately considered as discrete or continuous. The most celebrated ones include the Polya walk on a lattice and continuous-time random walk (CTRW) [3]. RW is such a natural construction that it has altogether been used across the whole realm of sciences. We refer the reader to [4] for an exposition of the probabilistic foundations of Brownian motion and RW, and to [5] for a discussion of a range of applications in the physical sciences.

In this paper we consider for definiteness discrete-time RW on lattices (or graphs in general). Within this context, RW is a Markov chain which describes the stochastic trajectory of a particle (random walker) taking successive random steps. For instance, in the well-known case of the Polya walk on a lattice, at each time step the particle jumps at random onto one of the neighboring nodes. The walk thus generates a random path on the lattice.

The relationship between RW and the statistics and entropy of paths is the main thread of this paper. In Section 2 we review various features of the statistics of paths. We recall how to count paths by means of the adjacency matrix A of a graph. We then present the relationship between RW and path integrals. The Feynman path-integral formalism [6] for a free particle, where trajectories are weighted only by their length, suggests that all paths of given length and endpoints should be equally probable. At variance with this picture, the field-theoretical approach to a relativistic particle propagating in a curved background requires that paths of the same length are not equally probable, but rather that their statistical weights depends on the nodes through which they pass. Both formalisms only agree in the particular case of k-regular graphs, where all the nodes have the same degree. Section 3 is devoted to RW models on an arbitrary graph. The main emphasis is put on two different canonical ways of defining RW, namely generic

random walk (GRW) and maximal entropy random walk (MERW), respectively corresponding to the field-theoretical and path-integral formalisms. In generic random walk (GRW), the particle sitting at a node of degree k jumps onto any neighboring node with uniform probability $1/k$, maximizing thus the entropy production locally, albeit not globally. In the stationary state, the probability π_a of finding the particle at node a is proportional to the degree k_a. When the lattice is regular (*i.e.*, all nodes have the same degree), all paths of a given length between two given points are equally probable, and thus have maximal entropy. Nevertheless, in accord with the field-theoretical formalism, as soon as the graph is not regular GRW trajectories are no longer equally probable.

We then turn to maximal entropy random walk (MERW). This novel kind of RW has been put forward and investigated by us in a recent work [7]. It is defined in such a way as to ensure that all paths of given length and endpoints are equally probable, in accord with the Feynman path integral. In other words, MERW is meant to maximize entropy globally, albeit not locally. It is still a Markov (memoryless) process, defined by local but non-trivial rules involving the largest eigenvalue of the adjacency matrix of the graph and the associated Perron-Frobenius eigenvector. The latter appears as the ground state of a quantum-mechanical tight-binding Hamiltonian, where the nodes a whose degree k_a is smaller than the maximal degree $k_{\max}$ carry a repulsive site potential $V_a = k_{\max} - k_a$. In the stationary state, the probability π_a of finding the particle at node a is given by the square of the component ψ_{1a} of the Perron-Frobenius eigenvector. As a byproduct, we introduce three definitions of the effective degree of a graph. The connection between RW, and especially GRW and MERW, and stochastic quantization is then made in Section 4.

In the rest of the paper we make a comparative investigation of GRW and MERW. A variety of examples of finite graphs are dealt with in Section 5, including bipartite and linear graphs. Section 6 is devoted to extended one-dimensional structures (ladder graphs). As a general rule, the effect of the repulsive potential on a particle performing MERW extends over the whole system. We consider successively the situation of one or two repulsive impurities, the converse situation of an attractive impurity where the stationary distribution is carried by a localized impurity state, and the case of a weakly diluted graph, obtained by removing a small fraction of bonds at random. The higher-dimensional situation is illustrated by several two-dimensional examples in Section 7. It is shown that MERW can lead to better transport properties than GRW, on the example of a non-bipartite two-dimensional lattice, the dual $(4, 8^2)$ lattice. In the case of weakly diluted lattices, obtained by removing a small fraction of bonds at random, it is shown that any small amount of disorder is sufficient to

localize the stationary state of MERW in the largest nearly spherical region which is free of defects. This unexpected localization effect takes place in any dimension. We provide a quantitative explanation for it in terms of a classical Lifshitz phenomenon.

The interested reader is referred to the interactive MATHEMATICA demonstration by one of us (BW) for many more illustrations of the unusual static and dynamical features of MERW [8].

2. Statistics of paths

2.1. Enumerating paths on a graph

A path is a very common object in graph theory (see, *e.g.*, [9], [10]). It is a finite sequence of adjacent (neighboring) nodes on a graph. Its length is defined as the number n of steps of the path. Each step follows a link (bond, edge) of the graph.

In this paper we consider only undirected graphs, *i.e.*, graphs whose edges have no orientation. We first recall how to enumerate paths $\{\gamma_{ba}(n)\}$ of length n going from node a to node b on a finite connected graph. Throughout this paper we use notations consistent with those used in QM: the initial (resp. final) state is the second (resp. first) index of transition matrices or propagators. The number $N_{ba}(n)$ of paths $\{\gamma_{ba}(n)\}$ can be calculated recursively as

$$N_{ba}(n+1) = \sum_c A_{bc} N_{ca}(n), \tag{2.1}$$

where $A = (A_{ab})$ is the adjacency matrix of the graph:

$$A_{ab} = \begin{cases} 1 & \text{if } a, b \text{ are neighbors,} \\ 0 & \text{otherwise.} \end{cases} \tag{2.2}$$

For a finite undirected graph with N nodes, A is a symmetric $N \times N$ matrix. We have

$$\sum_b A_{ab} = k_a, \tag{2.3}$$

where k_a denotes the degree (number of neighbors) of node a, and

$$\operatorname{tr} A^2 = \sum_a k_a = 2L, \tag{2.4}$$

where L is the number of links of the graph.

Applying the recursion relation (2.1) n times to the initial condition $N_{ba}(0) = \delta_{ba}$, where δ_{ba} is the Kronecker delta, one obtains

$$N_{ba}(n) = (A^n)_{ba} = \sum_i \psi_{ib}\psi_{ia}\lambda_i^n, \qquad (2.5)$$

where A^n is n-th power of the adjacency matrix, and ψ_i denote the normalized eigenvectors of A associated with the eigenvalues λ_i:

$$A\psi_i = \lambda_i\psi_i, \qquad \sum_a \psi_{ia}^2 = 1. \qquad (2.6)$$

The second index of ψ_{ia} denotes a-th component of ψ_i. The N eigenvalues are assumed to be ordered so as to have decreasing absolute values: $|\lambda_1| \geq |\lambda_2| \geq \dots$ In the large-n limit, the sum (2.5) is dominated by the largest eigenvalue λ_1 of the adjacency matrix.

After Boltzmann, Gibbs, and Shannon, the entropy $H_{ba}(n)$ of the ensemble of paths $\{\gamma_{ba}(n)\}$ is defined as the logarithm of the number of paths:

$$H_{ba}(n) = \ln N_{ba}(n). \qquad (2.7)$$

For $n \to \infty$, this entropy grows as

$$H_{ba}(n) \approx n \ln \lambda_1 + \ln(\psi_{1b}\psi_{1a}). \qquad (2.8)$$

The leading term is independent of the positions of the endpoints a, b. So, for large n, the entropy density per step (also called entropy production rate),

$$h = \lim_{n\to\infty} \frac{H_{ba}(n)}{n} = \ln \lambda_1, \qquad (2.9)$$

only depends on the largest eigenvalue λ_1 of the adjacency matrix A. The concept of entropy production can be generalized to a broader class of Markov chains, where the transition probabilities also depend on some field defined on the graph [11].

Under the mild hypothesis that the adjacency matrix A is *primitive* (or *regular*, see [12]), it follows from the Perron-Frobenius theorem that λ_1 is positive, whereas all the other eigenvalues are strictly smaller in modulus, and that the corresponding eigenvector ψ_1 can be chosen so as to have strictly positive components: $\psi_{1a} > 0$. In the present situation of undirected graphs, the matrix A is symmetric and its spectrum is real. The primitiveness hypothesis thus only excludes the case of bipartite graphs, which can be dealt with separately (see Section 5.2). For a bipartite graph, we have $\lambda_2 = -\lambda_1$, and hence $N_{ba}(n)$ oscillates with n, so that Eq. (2.8) possesses an additive oscillating contribution of order unity.

2.2. The path integral of a free relativistic particle

An interesting application of the statistics of paths is the description of a free relativistic particle. In the Feynman formulation of QM, quantum amplitudes are calculated as path integrals [6]. For a particle propagating in d-dimensional Minkowski spacetime, the amplitude is given as an integral over spacetime trajectories $x_{ba}(\tau)$ going from an initial spacetime point a to a final one b:

$$G_{ba} = \int [\mathrm{D}x_{ba}(\tau)] \; \mathrm{e}^{\frac{\mathrm{i}}{\hbar} S[x_{ba}(\tau)]}, \tag{2.10}$$

where $\hbar$ is Planck's constant. The action of a free scalar particle is $S = Mc \int_a^b \mathrm{d}s$, where $\mathrm{d}s^2 = (\mathrm{d}x^0)^2 - (\mathrm{d}\vec{x})^2$ is the spacetime interval, and M is the mass of the particle. The spacetime coordinates of point $x = (ct, \vec{x})$ will be denoted by x^μ ($\mu = 0, 1, \ldots, d-1$) and the speed of light as well as Planck's constant will be set to unity for convenience: $\hbar = c = 1$. One way of performing the integral (2.10) is to use the Wick rotation $(x^0, \vec{x}) \to (\mathrm{i}x^0, \vec{x})$ and to calculate a related quantity, called the Euclidean propagator (or Euclidean kernel). One then rotates the result back to the Minkowskian sector. Under Wick's rotation, the spacetime interval $\mathrm{d}s^2 = (\mathrm{d}x^0)^2 - (\mathrm{d}\vec{x})^2$ transforms to $-\mathrm{d}s^2 = -\left((\mathrm{d}x^0)^2 + (\mathrm{d}\vec{x})^2\right)$. The Euclidean propagator is defined by taking a proper branch of the square root of $\sqrt{-\mathrm{d}s^2}$:

$$G_{ba} = \int [\mathrm{D}x_{ba}(\tau)] \; \mathrm{e}^{-S[x_{ba}(\tau)]}, \tag{2.11}$$

where the free-particle action

$$S[x(\tau)] = M \int \mathrm{d}\tau \sqrt{\eta_{\mu\nu} \dot{x}^\mu \dot{x}^\nu} = M \int \mathrm{d}s \tag{2.12}$$

is proportional to the length of the corresponding Euclidean trajectory. Here $\eta = (\eta_{\mu\nu}) = \mathrm{diag}(1, \ldots, 1)$ denotes the Euclidean metric tensor and the Einstein summation convention is used. The trajectory $\tau \mapsto x(\tau)$ is parametrized by its proper time τ. The dots denote derivatives with respect to τ. The action $S[x(\tau)]$ is invariant with respect to diffeomorphic reparameterizations of the trajectory, so that the choice of parametrization does not play any role.

The Euclidean propagator (2.11) calls for a probabilistic interpretation, as the integrand is positive. A good way of emphasizing this feature is to use a lattice regularization. This is a standard strategy in field theory: one discretizes spacetime, calculates the propagator, and then takes the continuum limit by sending the lattice spacing to zero (see, *e.g.*, [13]). If one does this carefully, the outcome is independent of the discretization and all the symmetries of the underlying continuum theory are restored. Finally,

the results are rotated from the Euclidean sector back to the Minkowskian one. In order to show how this works, let us consider the case where the continuous spacetime $\mathbb{R}^d$ is discretized into the hypercubic lattice $\mathbb{Z}^d$, with lattice spacing ϵ. The integral over all possible trajectories from a to b in the Euclidean propagator (2.11) is replaced by a sum over all possible paths between a and b:

$$G_{ba} = \sum_{\{\gamma_{ba}\}} W(\gamma_{ba}) \, \mathrm{e}^{-\mu n[\gamma_{ba}]}, \tag{2.13}$$

where $\mu = M\epsilon$, $n[\gamma_{ba}]$ is the length of γ_{ba}, equal to the number of edges along this trajectory, and $W(\gamma_{ba})$ are statistical weights corresponding to the integration measure $[\mathrm{D}x_{ba}(t)]$ defining the ensemble of trajectories in Eq. (2.11). At variance with the non-relativistic case, in relativistic QM trajectories may go back and forth in the time direction. A trajectory which locally goes backward in time is interpreted as an antiparticle propagating forward in time. Turning points, where the trajectory changes its time direction, correspond to particle-antiparticle creation or annihilation events (see Figure 1).
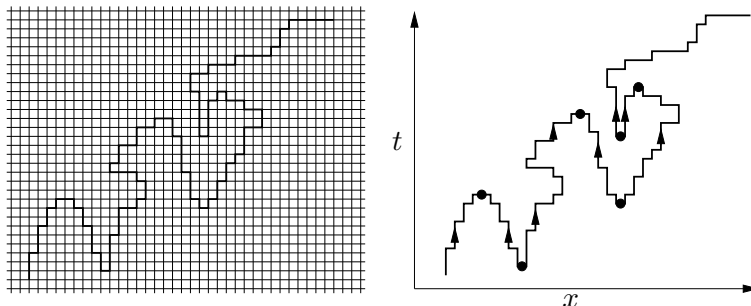

Fig. 1. Left: Example of a path on a 2D lattice. Right: the same path is interpreted as a trajectory of a relativistic quantum particle in (1+1)-dimensional spacetime. Arrows show the direction of time, whereas black circles are creation/annihilation events.

Now, an interesting question arises: how should the weights $\{W(\gamma_{ba})\}$ be chosen in order to obtain the *correct* relativistic Quantum Mechanics? The most natural choice consists in setting all $W(\gamma_{ba})$ to be equal. In other words, all the possible trajectories with a given length are assumed to be equally probable. Although this is the right prescription for paths on regular lattices, we shall see that this choice stands in contradiction with another formulation of QM if the underlying lattice is not regular. Yet, let us first consider the case where $W(\gamma_{ba}) = 1$. Eq. (2.13) can then be viewed as the

Laplace transform of the number of trajectories of length n,

$$
\begin{aligned}
G_{ba} &= \sum_n \mathrm{e}^{-\mu n} N_{ba}(n) = \sum_n \mathrm{e}^{-\mu n} (A^n)_{ba} \\
&= \left(\mathbb{1} - \mathrm{e}^{-\mu} A\right)^{-1}_{ba} = \sum_i \frac{\psi_{ib}\psi_{ia}}{1 - \mathrm{e}^{-\mu}\lambda_i},
\end{aligned}
\tag{2.14}
$$

where we denoted the identity matrix by $\mathbb{1} = (\delta_{ab})$. The Euclidean propagator is thus directly related to the statistics of paths, and to the adjacency matrix A. It has a first singularity (simple pole) for $\mu \to \ln \lambda_1$.

The generalization of the above construction to a curved spacetime is straightforward. In discrete quantum gravity models curved backgrounds are discretized using simplicial manifolds [14]. Such a manifold consists of equilateral d-simplices which are put together to form a d-dimensional manifold. In $d = 2$ dimensions we obtain an equilateral triangulation [15]. One can additionally impose a causal structure by introducing a foliation which singles out the temporal direction. This approach involving causal dynamical triangulations, referred to as Lorentzian simplicial gravity [16], is also extensively used to discretize path integrals in quantum gravity. The Euclidean action of a free particle in a curved background is

$$
S[x(\tau)] = M \int \mathrm{d}\tau \sqrt{g_{\mu\nu}\dot{x}^\mu \dot{x}^\nu} = M \int \mathrm{d}s,
\tag{2.15}
$$

where $g_{\mu\nu}$ is the metric tensor, so that the action is, as before, proportional to the length of trajectory. Assuming again weights $W(\gamma_{ba}) = 1$, the Euclidean propagator is given by the same formula (2.14) as in flat spacetime, except that now A is the adjacency matrix of the graph representing the non-trivial geometrical background in which the particle propagates. One can alternatively consider paths on a graph dual to the given simplicial manifold. This graph is k-regular with $k = d+1$. The corresponding paths pass through the centers of the simplices of the manifold.

2.3. Field-theoretical approach

Let us now discuss an alternative derivation of the Euclidean propagator. A free relativistic particle propagating in a given background can be described by a free field (see, e.g., [17]) with action

$$
S = \frac{1}{2} \int \mathrm{d}^d x \sqrt{g} \left(g^{\mu\nu} \frac{\partial \Phi}{\partial x^\mu} \frac{\partial \Phi}{\partial x^\nu} + M^2 \Phi^2 \right),
\tag{2.16}
$$

where $\Phi = \Phi(x)$ is a scalar field and $g_{\mu\nu} = g_{\mu\nu}(x)$ is the metric tensor at the spacetime point x. We consider here only the Euclidean sector, i.e., $g_{\mu\nu}$

having the Euclidean signature $(+, +, \ldots, +)$. The matrix $g^{\mu\nu}$ is the inverse of $g_{\mu\nu}$, and $g = \det(g_{\mu\nu})$. Integrating the first term by parts and assuming that boundary terms vanish, one obtains

$$S = \frac{1}{2} \int \mathrm{d}^d x \sqrt{g} \ \Phi \left(-\nabla^2 + M^2 \right) \Phi, \qquad (2.17)$$

where

$$\nabla^2 = \frac{1}{\sqrt{g}} \frac{\partial}{\partial x^\mu} \sqrt{g} g^{\mu\nu} \frac{\partial}{\partial x^\nu} \qquad (2.18)$$

is the Laplace-Beltrami operator. The Euclidean propagator is defined as the two-point correlation function

$$G(x, y) = \frac{1}{Z} \int [\mathrm{D}\Phi] \ \Phi(x)\Phi(y) \ \mathrm{e}^{-S}, \qquad (2.19)$$

where $Z = \int [\mathrm{D}\Phi] \, \mathrm{e}^{-S}$ and $[\mathrm{D}\Phi]$ is the integration measure for a scalar field in the given geometrical background. The meaning of the latter measure becomes clear if one discretizes the geometry, using an equilateral graph with fields $\{\phi_a\}$ located at the nodes. The integration measure is assumed to be a product measure $[\mathrm{D}\Phi] = \prod_a \mathrm{d}\phi_a$. This is the same kind of assumption as was made about the weights $\{W(\gamma_{ba})\}$ in Section 2.2. This assumption is validated by the fact that it leads to the same propagator as the one obtained from the Klein-Gordon equation of motion of the scalar field. The discretized action reads

$$S = \frac{1}{2} \sum_{ab} A_{ab}(\phi_a - \phi_b)^2 + \frac{m^2}{2} \sum_a k_a \phi_a^2, \qquad (2.20)$$

or, equivalently,

$$S = \frac{1}{2} \sum_{ab} \phi_a \left(-\Delta_{ab} + m^2 k_a \delta_{ab} \right) \phi_b, \qquad (2.21)$$

where k_a denotes the degree of node a, and

$$\Delta_{ab} = -k_a \delta_{ab} + A_{ab} \qquad (2.22)$$

is the topological (or graph) Laplacian. Note that the sign of this operator is opposite to that commonly used in graph theory. We use this sign convention because we want the graph Laplacian to become the Laplace operator in the continuum limit. As a consequence, all eigenvalues of this operator are non-positive. The correspondence between the dimensionless discretized quantities and those in the original continuum theory is

$\Phi(x) \leftrightarrow \epsilon^{1-d/2}\phi_a$, $M^2 \leftrightarrow \epsilon^{-2}m^2$, $\mathrm{d}^d x \sqrt{g} \leftrightarrow \epsilon^d k_a$, where ϵ is the lattice spacing. The Laplace-Beltrami operator is discretized as the lattice Laplacian: $\mathrm{d}^d x \sqrt{g} \nabla^2 \leftrightarrow \epsilon^{d-2}\Delta_{ab}$.

The discretized Euclidean propagator is given by the Gaussian integral

$$G_{ba} = \frac{1}{Z} \int \prod_c \mathrm{d}\phi_c \; \phi_b \phi_a \; \exp\left(-\frac{1}{2}\sum_{cd} \phi_c \left(-\Delta_{cd} + m^2 k_c \delta_{cd}\right) \phi_d\right), \quad (2.23)$$

which can be done explicitly:

$$G_{ba} = \frac{1}{\sqrt{k_b k_a}} \left(m^2 \mathbb{1} - \widehat{\Delta}\right)^{-1}_{ba} = \frac{e^{-\hat{\mu}}}{\sqrt{k_b k_a}} \widehat{G}_{ba}, \quad (2.24)$$

where

$$\widehat{G}_{ba} = \left(\mathbb{1} - e^{-\hat{\mu}}\widehat{A}\right)^{-1}_{ba}. \quad (2.25)$$

The normalized graph Laplacian $\widehat{\Delta}$ is defined by $\widehat{\Delta}_{ba} = \Delta_{ba}/\sqrt{k_b k_a}$, whereas $\widehat{A}$ is a matrix with entries $\widehat{A}_{ba} = A_{ba}/\sqrt{k_b k_a}$, and $\hat{\mu} = \ln(1 + m^2)$. The geometric series expansion of (2.25) yields powers of the matrix $\widehat{A}$ of the type $(\widehat{A}^n)_{ab}$, which are nonzero only if all the factors A_{cd} in the product represent adjacent edges of the graph. In other words, $(\widehat{A}^n)_{ba}$ generates paths on the graph, each with some statistical weight. We thus obtain

$$\widehat{G}_{ba} = \sum_n e^{-\hat{\mu}n}(\widehat{A}^n)_{ba} = \sqrt{k_b k_a} \sum_{\{\gamma_{ba}\}} e^{-\hat{\mu}n[\gamma_{ba}]} \prod_{c \in \gamma_{ba}} \frac{1}{k_c}. \quad (2.26)$$

Comparing Eqs. (2.14) and (2.26), we see that both approaches lead to different propagators for a free particle on a graph representing a discretized curved background. The main difference is the following. In Eq. (2.14) all paths have equal weights $W(\gamma_{ba}) = 1$, as they are just weighted by an exponential factor depending on the path's length, whereas in Eq. (2.26) paths have an additional weight $W(\gamma_{ba}) = \sqrt{k_b k_a} \prod_{c \in \gamma_{ba}} (1/k_c)$. Thus, the path-integral formulation which is consistent with the field-theoretical approach requires that paths of the same length are not equally probable, but rather that their statistical weights depends on the nodes through which they pass. In the particular case of k-regular graphs, *i.e.*, graphs for which all nodes have the same degree k, (2.14) and (2.26) are equivalent. Indeed, since the weights $W(\gamma_{ba}) = k^{-n[\gamma_{ba}]}$ only depend on the length of paths, the propagators can be mapped onto one another through $\mu = \hat{\mu} + \ln k$.

3. Random walks on a graph

So far we have discussed the statistics of paths and its relationship to path integrals. Another area where the statistics of paths naturally arises is random walk on graphs. Random walk is a stochastic process, providing a microscopic representation of diffusion, which describes a particle (or a gas of non-interacting particles) hopping between the nodes of a graph. One is interested in the probability $p_{ba}(\tau)$ that a particle, which was initially at node a, is at node b at the later time τ. We will consider only discrete-time random walks, such that the particle hops to a neighboring node of the graph at each time step. Graphs can be treated as a discretization of a geometrical background in which diffusion takes place. In this case one usually wishes to restore the continuum theory by sending the lattice spacing and the time interval to zero in a proper way (*diffusive scaling*). Graphs may also model real discrete structures. In this case there is no reason to invoke a continuum limit. For instance, complex networks are commonly used to model the Internet, the worldwide airline network, social networks, and so on [18]. In this context, random walk may describe the propagation of information, passengers, etc.

3.1. Generalities

Discrete-time random walk on a finite connected graph is an irreducible Markov chain. The stochastic motion of the particle is encoded in transition probabilities $\{P_{ba}\}$ that a particle sitting at node a will hop to node b at the next time step. One can collect the transition probabilities in a transition (or Markov) matrix $P = (P_{ba})$ (see [19]). The matrix P fulfills the conditions for being a stochastic matrix: the probabilities are non-negative ($P_{ba} \geq 0$), while the entries in each row sum up to unity: $\sum_b P_{ba} = 1$, ensuring the conservation of probability. We will only consider transition matrices which conform with the structure of the undirected graph, that is for any pair (a, b) of neighboring nodes we have $A_{ab} = A_{ba} = 1$, and $P_{ab} > 0$, $P_{ba} > 0$, although $P_{ab} \neq P_{ba}$ in general. All the other entries of P (including the diagonal ones) are zero, so that in a single time step the particle may only hop to a neighboring node.

Using the transition matrix P, one can write a recursive relation for the probabilities $p_{ba}(\tau)$:

$$p_{ba}(\tau + 1) = \sum_c P_{bc} p_{ca}(\tau), \qquad (3.1)$$

which is analogous to the combinatorial formula (2.1). Solving it with the initial condition $p_{ba}(0) = \delta_{ba}$, corresponding to the particle starting

at node a, one obtains

$$p_{ba}(\tau) = (P^\tau)_{ba}, \tag{3.2}$$

which is again analogous to Eq. (2.5). The interpretation of both formulas is different: (2.5) has a combinatorial meaning, while (3.2) has a probabilistic one. There is, however, a strong similarity between both problems, namely that they can be formulated in terms of path statistics. A particle performing a random walk on a graph marks a trajectory of consecutive nodes visited during the walk. The length n of this path is equal to the time (number of steps) τ of the random walk. Let $\gamma_{a_\tau a_0} = (a_\tau, \ldots, a_1, a_0)$ be a path of length τ from a_0 to a_τ. For fixed endpoints a_0 and a_τ, the probability that the path visits the given sequence of nodes reads

$$P(\gamma_{a_\tau a_0}) = P_{a_\tau a_{\tau-1}} \cdots P_{a_2 a_1} P_{a_1 a_0}. \tag{3.3}$$

The paths generated by the Markov chain representing the random walk may thus have in general different statistical weights, in contrast to the combinatorial problem where each path is counted with the same weight, independently of the intermediate nodes.

One case of much interest is generic (ordinary) random walk (GRW), generalizing the Polya walk on a lattice, which will be investigated in Section 3.3. Neighbors are selected uniformly at each time step, $i.e.$, $P_{ba} = A_{ba}/k_a$, and hence

$$P(\gamma_{a_\tau a_0}) = \prod_{i=0}^{\tau-1} \frac{1}{k_{a_i}}, \tag{3.4}$$

which is the same weight as in (2.26). Therefore, the trajectories entering the field-theoretical derivation of path integrals are the same as those generated by GRW. For GRW on k-regular graphs, there is a simple correspondence between the combinatorial result (2.5) and the probabilistic one (3.2). One can interpret $N_{ba}(n)/k^n$ as the probability $p_{ba}(\tau)$ of reaching node b after $\tau = n$ steps, starting from a, since the numerator $N_{ba}(n)$ is the number of paths of length n between a and b, while the denominator k^n is the number of paths of length n starting from a and ending anywhere.

A natural question arises: *Can one find a stochastic matrix which generates trajectories between given endpoints with uniform weights, irrespective of intermediate nodes, for an arbitrary (non-regular) graph?* In other words: *Is there a random walk such that all trajectories between two given endpoints are equally probable?* A positive answer to the above question is provided by maximal entropy random walk (MERW), to be investigated in Section 3.4.

Before this, let us recall some basic properties of the Markov chain defined by the transition matrix P. As already mentioned, we will restrict ourselves to the situation where the transition matrix is primitive. In this

case, the probability distribution $p_{ba}(\tau)$ tends to a limiting distribution $\lim_{\tau \to \infty} p_{ba}(\tau) = \pi_b$, independently of the initial point a. This unique distribution is given by the normalized left eigenvector of the stochastic matrix corresponding to unit eigenvalue:

$$\pi_b = \sum_a P_{ba} \pi_a, \qquad \sum_a \pi_a = 1. \tag{3.5}$$

3.2. The entropy of a random walk

Let us denote by $P(a_\tau, \ldots, a_1, a_0)$ the probability that a random walker follows a path $a_0 \to a_1 \to \ldots \to a_\tau$. The Markov property expressed by the master equation (3.1) implies that this probability reads

$$P(a_\tau, \ldots, a_1, a_0) = P_{a_\tau a_{\tau-1}} \ldots P_{a_2 a_1} P_{a_1 a_0} \pi_{a_0}(0), \tag{3.6}$$

where $\pi(0)$ is the probability distribution of the initial point.

We define the entropy H_τ of the ensemble of paths of length τ as:

$$H_\tau = - \sum_{a_0, a_1, \ldots, a_\tau} P(a_\tau, \ldots, a_1, a_0) \ln P(a_\tau, \ldots, a_1, a_0), \tag{3.7}$$

where the sum effectively runs over all the allowed paths of length τ generated by the master equation (3.1). Inserting Eq. (3.6) into (3.7), we find that the entropy is asymptotically produced at a constant rate, $h_{\mathrm{RW}} = \lim_{\tau \to \infty}(H_\tau/\tau)$, which reads

$$h_{\mathrm{RW}} = - \sum_a \pi_a \sum_b P_{ba} \ln P_{ba}, \tag{3.8}$$

independently of the initial distribution $\pi(0)$. This means that after a long time, when the process has reached its stationary state, the entropy production rate is equal to a local production rate, $h_a = - \sum_b P_{ba} \ln P_{ba}$, averaged over π_a. The stationary distribution π_a is itself entirely determined by the stochastic matrix P defining the random walk (see Eq. (3.5)), and so is the entropy production rate (3.8).

In the following we shall compare the entropies of two different types of random walk: generic random walk (GRW), which locally maximizes entropy production, as already mentioned earlier, and maximal entropy random walk (MERW), which maximizes entropy globally.

3.3. Generic random walk (GRW)

Generic random walk (GRW), generalizing the Polya walk on a lattice, has already been defined above Eq. (3.4). The particle sitting at node a

with degree k_a hops to one of the neighboring nodes b without giving a preference to any of them, *i.e.*, with probability $1/k_a$, so that

$$P_{ba} = \frac{A_{ba}}{k_a}. \tag{3.9}$$

This maximally random choice at each time step corresponds to a local maximization of the entropy production. The local entropy $h_a = -\sum_b P_{ba} \ln P_{ba}$ is indeed maximized for the uniform selection of neighbors (3.9). One may ask whether this choice also maximizes the entropy production rate h_{RW} (3.8) of entire paths. We expect that it does not, because the statistical weights of paths for GRW are given by Eq. (3.4) and hence paths are not equally probable in general, even if they have identical length and endpoints (see Figure 2).
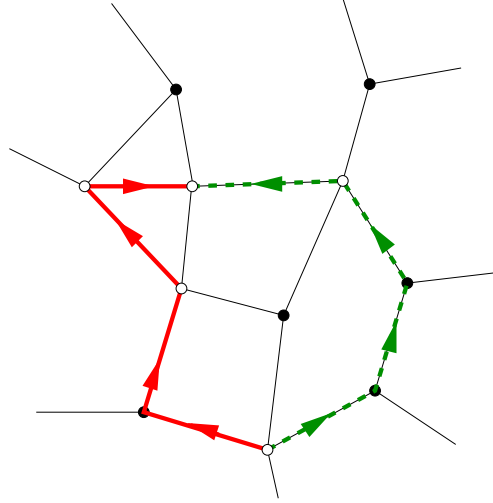
Fig. 2. (Color online). Two paths (solid and dashed line) on a graph with the same endpoints and length, but different statistical weights in GRW, because they pass through different nodes. Skipping probabilities attached to the endpoints, the solid path has probability $1/4 \cdot 1/3 \cdot 1/4 \cdot 1/4 = 1/192$, whereas the dashed one has probability $1/4 \cdot 1/3 \cdot 1/3 \cdot 1/4 = 1/144$.

The stationary distribution π_a obtained from (3.5) for GRW reads

$$\pi_a = \frac{k_a}{2L}. \tag{3.10}$$

The stationary probabilities of GRW are *directly* proportional to the node degrees. This is to be contrasted with Eq. (3.4), which states that the

contribution of intermediate nodes to the weight of a given path is *inversely* proportional to their degrees.

Inserting Eq. (3.10) into (3.8), we find the entropy production rate h_{GRW} of generic random walk in the form:

$$h_{\text{GRW}} = \frac{1}{2L} \sum_a k_a \ln k_a. \tag{3.11}$$

3.4. Maximal entropy random walk (MERW)

We now turn to the question raised in Section 3.1. If there is a random walk which maximizes entropy, we expect that all paths of given length between two given endpoints will be equally probable. The weights of paths may however still depend on the endpoints, as the contribution of endpoints will eventually disappear in the limit $\tau \to \infty$, as it did in Eq. (2.9). We are therefore looking for a stochastic matrix P such that the weight (3.3) is a function of length τ and endpoints a, b only. Moreover, as we expect that the matrix P should have entropy $h = \ln \lambda_1$, the construction must somehow be related to the largest eigenvalue of the adjacency matrix.

It can be checked that maximal entropy random walk (MERW) [7], defined by the following transition probabilities:

$$P_{ba} = \frac{A_{ba}}{\lambda_1} \frac{\psi_{1b}}{\psi_{1a}}, \tag{3.12}$$

fulfills all the requirements. First, P is a stochastic matrix. The components ψ_{1a} of the eigenvector corresponding to the largest eigenvalue λ_1 are all positive, by virtue of the Perron-Frobenius theorem. One can check that the row sums are equal to unity: $\sum_b P_{ba} = 1$. Finally, MERW conforms with the graph structure.

The stationary distribution (3.5) for MERW can be checked to be given by the squared components of the normalized eigenvector ψ_1:

$$\pi_a = \psi_{1a}^2, \tag{3.13}$$

so that the L^1 normalization (3.5) of the π_a nicely matches the L^2 normalization (2.6) of the ψ_{ia}. Inserting the above result into (3.8), we obtain an expression for the entropy production rate,

$$h_{\text{MERW}} = \ln \lambda_1 = h, \tag{3.14}$$

which indeed coincides with the combinatorial entropy of paths (2.9). It can also be checked that the statistical weight (3.3) for a path $\gamma_{a_\tau a_0} =$

$(a_\tau, \ldots, a_1, a_0)$ is independent of intermediate nodes. Indeed, inserting (3.12) into (3.3), we obtain

$$P(\gamma_{a_\tau a_0}) = \frac{1}{\lambda_1^\tau} \frac{\psi_{1a_\tau}}{\psi_{1a_0}}. \tag{3.15}$$

This expression only depends (exponentially) on the path length τ, and on the endpoints a_0 and a_τ, through the components of ψ_1. This means that all paths of length τ from a_0 to a_τ are indeed equally probable. In other words, the probability measure on this ensemble of paths is uniform, and the corresponding entropy is maximal.

To the best of our knowledge, MERW has been introduced and studied for the first time in our recent work [7] in the context of random walk and path integrals. However, the construction of stochastic processes with maximal entropy in the framework of information theory is much older, as it dates back to Shannon [20]. The concept has been formalized by Parry [21] as intrinsic Markov chains. In the context of ergodic theory, the stationary distribution (3.13) is referred to as a Shannon-Parry measure [22], whereas yet other related matters are discussed in Refs. [23] and [24].

The Perron-Frobenius eigenvector ψ_1 can be interpreted as the ground state of the Hamiltonian $H = (H_{ab})$, with $H_{ab} = k_{\max}\delta_{ab} - A_{ab} = -\Delta_{ab} + V_a\delta_{ab}$, where $V_a = k_{\max} - k_a$, and $k_{\max}$ is the maximal node degree in the graph. In other words, ψ_1 is the ground-state wavefunction of the tight-binding equation

$$(H\psi_i)_a = (-\Delta\psi_i)_a + V_a\psi_{ia} = E_i\psi_{ia}, \tag{3.16}$$

with

$$V_a = k_{\max} - k_a, \quad E_i = k_{\max} - \lambda_i, \tag{3.17}$$

and the stationary distribution (3.13) is the square of this ground-state wavefunction. The potential V_a is non-negative. It is positive (*i.e.*, repulsive) for nodes whose degree is smaller than $k_{\max}$ — the smaller the degree, the larger the repulsion. All the eigenvalues E_i of H are clearly non-negative, the ground-state eigenvalue $E_1 = k_{\max} - \lambda_1$ being the smallest one. For a k-regular graph, the potential vanishes identically. The Hamiltonian H thus describes the propagation of a free particle. The ground-state energy is $E_1 = 0$ and we have $\psi_{1a} = 1/\sqrt{N}$, so that $\pi_a = 1/N$, where N is the number of nodes of the graph. Hence the stationary measure π_a is uniform over the k-regular graph.

3.5. Effective degrees

It is interesting to illustrate the above considerations by associating effective degrees to the entropies of GRW and of MERW on a graph. Consider

an arbitrary finite graph whose N nodes ($a = 1, \ldots, N$) have degrees k_a. We introduce the following three definitions of its effective degree:

- The first effective degree of a graph is simply its mean degree,

$$K_1 = \frac{1}{N} \sum_a k_a = \frac{2L}{N}. \tag{3.18}$$

 The node degrees k_a indeed sum up to twice the number of links L (see (2.4)).

- The second definition is the GRW-based degree $K_2 = \exp(h_{\mathrm{GRW}})$, where the entropy h_{GRW} of GRW is given by (3.11), hence

$$K_2 = \exp\left(\frac{1}{2L} \sum_a k_a \ln k_a\right) = \left(\prod_a k_a^{k_a}\right)^{1/(2L)}. \tag{3.19}$$

- The third one is the MERW-based degree $K_3 = \exp(h_{\mathrm{MERW}})$, where the entropy h_{MERW} of MERW is given by (3.14), hence

$$K_3 = \lambda_1. \tag{3.20}$$

The intuition behind the entropic definitions of the effective node degrees K_2 and K_3 is the following. On a k-regular graph, the number of paths of length n starting from a given node grows as $N(n) = k^n$, so that the degree k is related to the entropy production rate as $k = \exp(h)$. A natural extension of this relation to irregular graphs leads to (3.19) or (3.20) if one uses the local or global rule for maximal entropy production, respectively.

The three definitions of the effective degree yield in general different values. Their number-theoretical natures are very different: K_1 is a rational number, whereas K_2 is a fractional power of an integer, and K_3 is a solution of an algebraic equation of degree at most N. The effective degrees obey the inequalities

$$k_{\min} \leq K_1 \leq K_2 \leq K_3 \leq k_{\max}, \tag{3.21}$$

where $k_{\min}$ and $k_{\max}$ are the minimal and maximal values of the node degrees. The first and fourth of these inequalities are obvious, whereas the third one just expresses that MERW indeed has maximal entropy, and the second one originates in the convexity of the free energy

$$F(\beta) = \ln \sum_a k_a^\beta. \tag{3.22}$$

We have indeed $\ln K_2 = F'(1) \geq \ln K_1 = F(1) - F(0)$.

4. Stochastic quantization

As already mentioned, the trajectories generated by a random walk can be used to define quantum amplitudes. In this section we make this statement more precise within the framework of stochastic quantization (see, *e.g.*, [17]). As one can anticipate, MERW will reproduce the path-integral propagator (2.13), and GRW the field-theoretical propagator (2.26).

Let us start with MERW. We consider paths generated by the stochastic matrix (3.12), and restrict ourselves to equilibrium paths, initiated from the stationary state (3.13). The probability of such a path is

$$P_{\text{eq}}(\gamma_{a_\tau a_0}) = P(a_\tau, \ldots, a_1, a_0)\pi_{a_0} = \mathrm{e}^{-\tau h}\psi_{1a_\tau}\psi_{1a_0}, \qquad (4.1)$$

with $h = \ln \lambda_1$, as one can see by multiplying (3.15) by $\psi_{1a_0}^2$. Keeping endpoints $a_0 = a$ and $a_\tau = b$ fixed and summing over intermediate states $a_1, \ldots, a_{\tau-1}$, we obtain a sum over all paths $\gamma_{ba}(\tau)$ from a to b of length τ:

$$\sum_{\{\gamma_{ba}\}} P_{\text{eq}}(\gamma_{ba}) = \sum_{a_{\tau-1}\ldots a_1} P_{\text{eq}}(b, a_{\tau-1}, \ldots, a_1, a) = N_{ba}(\tau)\mathrm{e}^{-\tau h}\psi_{1b}\psi_{1a}. \quad (4.2)$$

If we now multiply both sides by an additional exponential weight $\mathrm{e}^{-\hat{\mu}\tau}$ with a positive parameter $\hat{\mu} > 0$, and sum over all integer values of τ from zero to infinity, we eventually obtain

$$\sum_{\tau} \mathrm{e}^{-\hat{\mu}\tau} \sum_{\{\gamma_{ba}(\tau)\}} P_{\text{eq}}(\gamma_{ba}(\tau)) = \psi_{1b} G_{ba} \psi_{1a}, \qquad (4.3)$$

where G_{ba} is the propagator derived in the path-integral formalism (2.14) with $\mu = \hat{\mu} + h$. The above expression becomes singular as the sum diverges for $\hat{\mu} \to 0$, *i.e.*, $\mu \to h = \ln \lambda_1$. This situation describes the limit of a massless particle, in which all paths of any length are equally probable. The right-hand side of Eq. (4.3) has a characteristic sandwich form where G_{ab} stands between wave functions representing external states $\psi_{1a} = \sqrt{\pi_a}$ (see (3.13)).

We can now repeat the same construction for GRW with the stochastic matrix (3.9). As in the previous case, it is convenient to define a state function $\hat{\psi}$ as the square root of the stationary probability (3.10): $\hat{\psi}_a = \sqrt{\pi_a} = \sqrt{k_a/(2L)}$. The probability of an equilibrium path reads

$$P_{\text{eq}}(\gamma_{a_\tau a_0}) = P(a_\tau, \ldots, a_1, a_0)\pi_{a_0} = \hat{\psi}_{a_\tau}\hat{\psi}_{a_0}\sqrt{k_{a_\tau}k_{a_0}}\prod_{i=0}^{\tau}\frac{1}{k_{a_i}}, \qquad (4.4)$$

as one can see by multiplying (3.4) by (3.10). Applying the same procedure as for MERW, we obtain

$$\sum_{\tau=0}^{\infty} e^{-\hat{\mu}\tau} \sum_{\{\gamma_{ba}(\tau)\}} P_{eq}(\gamma_{ba}(\tau)) = \hat{\psi}_b \widehat{G}_{ba} \hat{\psi}_a, \qquad (4.5)$$

where $\widehat{G}_{ba}$ is equal to the field-theoretical propagator (2.26). As already mentioned, the two propagators are identical only for k-regular graphs. In this case, the largest eigenvalue of the adjacency matrix is $\lambda_1 = k$, the entropy rate is $h = \ln k$, $\mu = \hat{\mu} + \ln k$, $\hat{\psi}_a = \psi_{1a} = \sqrt{k/(2L)}$, and the stochastic matrix of MERW (3.12) is identical to that of GRW (3.9).

Let us conclude this section with a remark on the relationship with non-relativistic Quantum Mechanics. In the relativistic case discussed so far, the parameter τ was treated as *proper* time. The Euclidean propagators, either in the path-integral approach (4.3) or in the field-theoretical formalism (4.5), were independent of τ, since the latter variable was summed over. One can, however, treat τ as a universal time in a non-relativistic spacetime, and view the graph (or lattice) as a discretization of space only, hence skipping the summation over τ. This leads to a non-relativistic propagator for $(d+1)$-dimensional QM:

$$\sum_{\{\gamma_{ba}(\tau)\}} P_{eq}(\gamma_{ba}(\tau)) = \psi_{1b} K_{ba}(\tau) \psi_{1a}, \qquad (4.6)$$

where $K_{ba}(\tau)$ (or alternatively $\widehat{K}_{ba}(\tau)$) is defined as a sum over trajectories of fixed length τ. The non-relativistic propagator is thus related to the Euclidean relativistic propagator by a Laplace transform:

$$G_{ba}(\hat{\mu}) = \sum_{\tau} K_{ba}(\tau) e^{-\hat{\mu}\tau}. \qquad (4.7)$$

One can also explicitly add a time direction to the discretized theory by stacking d-dimensional lattices on top of each other. Doing so, one obtains a $(d+1)$-dimensional foliated lattice whose time slices are identical clone copies of d-dimensional space. In this context, the trajectories of a particle form directed polymers, which never go backward in time (see Figure 3). Thus MERW generates maximally entropic directed polymers which are equally probable in an ensemble of polymers having fixed endpoints. This is not the case for directed polymers generated by GRW in a curved background, discretized as a non-regular lattice.

5. Examples of finite graphs

In what follows we discuss properties of the stationary state for GRW and MERW on various finite graphs.
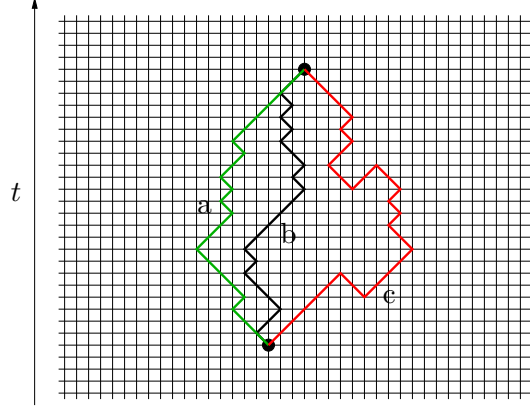
Fig. 3. (Color online). Trajectories of a non-relativistic particle on a (1+1)-dimensional square lattice form directed polymers (a,b), whereas trajectories which turn back in time are excluded (c). Both (a) and (b) have the same length and hence they are equally probable within the MERW (path-integral) formalism.

5.1. k-regular graphs

As already mentioned, the simplest situation is that of a k-regular graph, where all the nodes have the same degree k. Both GRW and MERW are defined by the uniform transition probabilities $P_{ba} = 1/k$ if nodes a and b are neighbors. The two processes therefore coincide, no matter how complicated the topology of the graph is. The corresponding stationary distribution is uniform: $\pi_a = 1/N$ for all nodes. We have consistently

$$K_1 = K_2 = K_3 = k. \tag{5.1}$$

5.2. Bipartite graphs

The next case, in order of increasing complexity, is that of bipartite graphs. We will consider the class of finite bipartite graphs such that all nodes in one subset of the graph have identical degree k_1, while in the other subset all nodes have degree k_2. The numbers of nodes of each type are then $N_1 = L/k_1$ and $N_2 = L/k_2$, where L denotes the number of links. For both GRW and MERW, the transition probabilities take two values: $P_{21} = 1/k_1$ (if node a has degree k_1 and node b has degree k_2) and $P_{12} = 1/k_2$ (if node a has degree k_2 and node b has degree k_1). The two processes therefore again coincide. The largest eigenvalue of the adjacency matrix is $\lambda = \sqrt{k_1 k_2}$. The corresponding eigenvector obeys $\psi_1 : \psi_2 = \sqrt{k_1} : \sqrt{k_2}$. The stationary distribution takes two values: $\pi_1 = k_1/(2L)$ and $\pi_2 = k_2/(2L)$. The effective

degrees read

$$K_1 = \frac{2k_1 k_2}{k_1 + k_2}, \qquad K_2 = K_3 = \sqrt{k_1 k_2}. \qquad (5.2)$$

In other words, K_1 is the harmonic mean of both degrees, whereas K_2 and K_3 coincide with their geometric mean. These results hold irrespective of the size and topology of the graph.

The first non-trivial example of a bipartite but non-regular graph corresponds to $k_1 = 2$ and $k_2 = 3$. We have $K_1 = 12/5 = 2.4$, whereas $K_2 = K_3 = \sqrt{6} = 2.449490$. These two values are different, albeit very close to each other.

5.3. The barred-square graph

The barred-square graph shown in Figure 4 is the simplest example of interest of a non-bipartite graph.
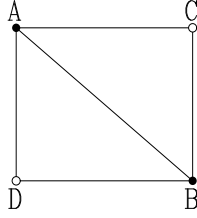
Fig. 4. The barred-square graph.

For GRW on this graph, the stationary distribution reads

$$\pi_A = \pi_B = \frac{3}{10}, \qquad \pi_C = \pi_D = \frac{1}{5}, \qquad (5.3)$$

so that we have $h_{\text{GRW}} = (\ln 108)/5$. The largest eigenvalue of the adjacency matrix is $\lambda = (\sqrt{17} + 1)/2$. The corresponding eigenvector obeys $\psi_A : \psi_C = (\sqrt{17} + 1) : 4$. Therefore, the stationary distribution for MERW reads

$$\pi_A = \pi_B = \frac{\sqrt{17} + 1}{4\sqrt{17}} = 0.310634, \quad \pi_C = \pi_D = \frac{\sqrt{17} - 1}{4\sqrt{17}} = 0.189366. \quad (5.4)$$

Finally, the effective degrees are

$$K_1 = \frac{5}{2} = 2.5, \quad K_2 = 108^{1/5} = 2.550849, \quad K_3 = \frac{\sqrt{17} + 1}{2} = 2.561553. \qquad (5.5)$$

These three values are again very close to each other.

5.4. Linear graphs

Consider now the family of linear graphs made of $N \geq 3$ nodes, as shown in Figure 5 for $N = 7$.
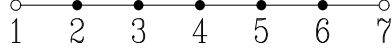

Fig. 5. The linear graph with $N = 7$ nodes.

The endpoints ($n = 1$ and $n = N$) have degree 1, whereas the $N - 2$ inner points ($n = 2, \ldots, N - 1$) have degree 2. The mean degree thus reads

$$K_1 = \frac{2(N - 1)}{N}. \tag{5.6}$$

For GRW on the linear graph, the stationary distribution is

$$\pi_1 = \pi_N = \frac{1}{2(N - 1)}; \qquad \pi_n = \frac{1}{N - 1} \qquad (n = 2, \ldots, N - 1), \tag{5.7}$$

and we have

$$K_2 = 2^{(N-2)/(N-1)}. \tag{5.8}$$

For MERW the stationary distribution is

$$\pi_n = \frac{2}{N} \sin^2 \frac{n\pi}{N + 1} \tag{5.9}$$

and we have

$$K_3 = \lambda = 2 \cos \frac{\pi}{N + 1}. \tag{5.10}$$

As the linear graph gets larger ($N \to \infty$), the three effective degrees converge to the limiting value 2, characteristic of the infinite chain, albeit at different rates:

$$K_1 = 2 - \frac{2}{N}, \quad K_2 = 2 - \frac{2 \ln 2}{N} + \cdots, \quad K_3 = 2 - \frac{\pi^2}{N^2} + \cdots \tag{5.11}$$

The positive differences $K_2 - K_1$, $K_3 - K_2$, and $K_3 - K_1$ are respectively maximal for $N = 4$, 9, and 6.

Figure 6 shows a comparison of the stationary distributions of GRW (5.7) and MERW (5.9) on the linear graph with $N = 29$ nodes. The effect of the endpoint impurities is strictly local in the case of GRW, as it only affects the distribution at the endpoints themselves. On the contrary, in the case of MERW we observe a non-local effect of the endpoints on the stationary distribution, which varies smoothly at the scale of the whole graph.
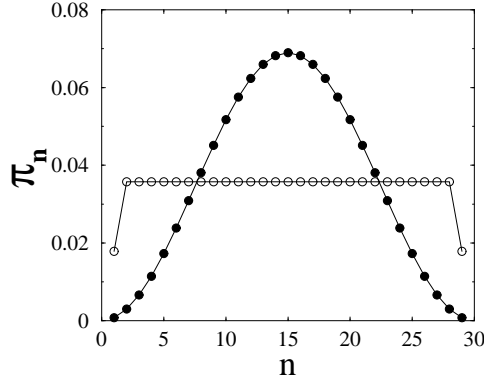
Fig. 6. The stationary distributions (5.7) of GRW (empty symbols) and (5.9) of MERW (filled symbols) on the linear graph with $N = 29$ nodes.

Rather paradoxically, the MERW-based effective degree K_3 converges as $1/N^2$, whereas the other two have a slower linear convergence in $1/N$.

The above picture is generic. Statistical properties of MERW may differ drastically from those of GRW. We recall that the stationary distribution for MERW is the square of the ground-state wavefunction of the Hamiltonian involved in the tight-binding equation (3.16). The latter describes the motion of a QM particle in the presence of a repulsive potential $V_a = k_{\max} - k_a$, supported by the impurity nodes whose degree is smaller than $k_{\max}$. These impurities can be expected to generate strong, non-local effects.

6. One-dimensional examples: ladders

We now turn to the investigation of MERW on extended structures, starting from quasi one-dimensional systems — ladder graphs. The full graph consists of two symmetric closed chains of nodes connected by rungs (see Figure 7). It is a 3-regular graph on which, as we have learned, GRW and MERW coincide.
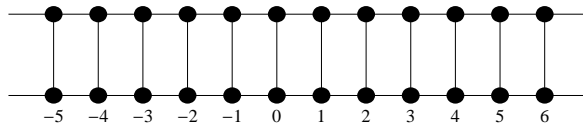
Fig. 7. The full ladder. Periodic boundary conditions along the chains are assumed.

In order to meet cases where MERW behaves in a non-trivial manner,

we remove some of the rungs [7]. Since the ground state is not degenerate and its wavefunction is expected to be symmetric w.r.t. the exchange of both lines of the ladder, it is sufficient to consider the tight-binding equation (3.16) in the symmetric sector. This equation takes the form

$$2\psi_{1a} - \psi_{1a-1} - \psi_{1a+1} + V_a\psi_{1a} = E_1\psi_{1a}, \qquad (6.1)$$

where $E_1 = 3 - \lambda_1$ and

$$V_a = \left\{ \begin{array}{ll} 0 & \text{if the rung at position } a \text{ is present,} \\ 1 & \text{if the rung at position } a \text{ is absent.} \end{array} \right. \qquad (6.2)$$

For definiteness we consider ladders whose length (circumference) is an even number $2N$. We will index nodes in each line by $a = -N, \ldots, N$, and impose periodic boundary conditions by identifying nodes N and $-N$.

6.1. A single impurity

Let us first create a single impurity at the origin by removing the rung at node $a = 0$ (see Figure 8).
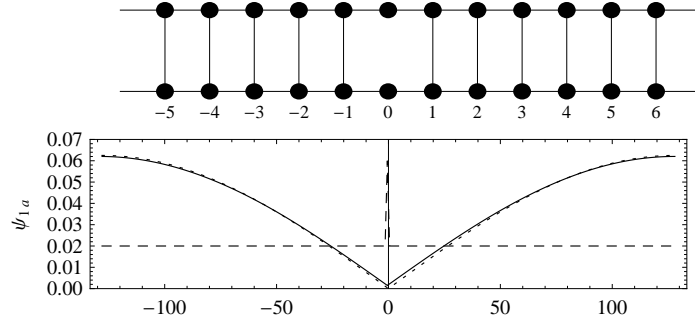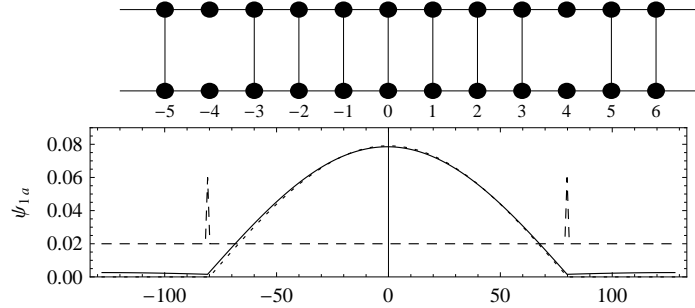

Fig. 8. Top: a ladder with one rung at $a = 0$ removed. Bottom: Plot of the numerically obtained ground-state wavefunction ψ_{1a} for $N = 128$ (solid line) compared with (6.5) (dotted line). The impurity potential V_a is also shown (dashed line, rescaled).

The potential $V_a = \delta_{a0}$ is concentrated on the impurity. Setting $E_1 = 2(1 - \cos q)$, *i.e.*, $\lambda_1 = 1 + 2\cos q$, with some unknown wavevector q, the (unnormalized) wavefunction reads

$$\psi_{1a} = \cos((N - |a|)q). \qquad (6.3)$$

The matching condition on the impurity yields the quantization condition

$$2\sin q \, \tan(Nq) = 1. \qquad (6.4)$$

The ground state corresponds to the smallest positive solution q to the latter equation. In the most interesting situation, namely for large N, we have $q \approx \pi/(2(N+2))$, and hence

$$\psi_{1a} \approx \frac{1}{\sqrt{2N}} \sin \frac{(|a|+2)\pi}{2N}. \tag{6.5}$$

The presence of a single defect has a non-local effect on the stationary probability distribution. The latter distribution is maximal at $a = N$, *i.e.*, at the node farthest from the removed rung, whereas it is minimal on the impurity. Although the potential is concentrated at a single node, it exerts a strong repulsion on a particle performing MERW. The situation is somewhat similar to that of long linear graphs, described in Section 5.4, where the endpoints of the finite linear chain acted as impurities whose effect was already non-local.

6.2. Two impurities

We now consider what happens when two rungs are removed at positions $a = n$ and $a = -n$ (see Figure 9).

Fig. 9. Top: a ladder with two rungs at $a = -n$ and $a = n$ removed, for $n = 4$. Bottom: Plot of the numerically obtained ground-state wavefunction ψ_{1a} for $N = 128$ and $n = 80$ (solid line) compared with (6.9) (dotted line). The impurity potential V_a is also shown (dashed line, rescaled).

The impurity potential $V_a = \delta_{a,n} + \delta_{a,-n}$ and the ground-state wavefunction are again symmetric in a. The (unnormalized) wavefunction reads

$$\psi_{1a} = \begin{cases} \cos((N-n)q) \, \cos(aq) & (-n \leq a \leq n), \\ \cos((N-|a|)q) \, \cos(nq) & (n \leq |a| \leq N). \end{cases} \tag{6.6}$$

The matching condition on the impurity yields the quantization condition

$$\sin q \, (\tan(nq) + \tan((N-n)q)) = 1. \tag{6.7}$$

For large N and n, the smallest solution reads approximately

$$q_1 \approx \min\left(\frac{\pi}{2n}, \frac{\pi}{2(N-n)}\right). \tag{6.8}$$

The ground-state wavefunction, and therefore the stationary distribution of MERW, essentially live on the larger part of the ladder which is free of defects. For $n > N/2$, this larger region is the central one. The ground-state wavefunction is well approximated by

$$\psi_{1a} \approx \begin{cases} \dfrac{1}{\sqrt{2n}} \cos \dfrac{a\pi}{2n} & (-n \leq a \leq n), \\ 0 & \text{otherwise.} \end{cases} \tag{6.9}$$

6.3. A single attractive impurity

One can also consider the reverse situation of attractive defects, *i.e.*, nodes having a degree larger than average. The simplest example is provided by a "degenerate ladder" with a single rung at $a = 0$ (see Figure 10). The nodes at the endpoints of the rung have degree $k = 3$, whereas all other nodes have $k = 2$. In this case the impurity potential reads $V_a = 1 - \delta_{a0}$. It is everywhere repulsive, except at the origin. The ground state can thus be expected to be localized around the origin.
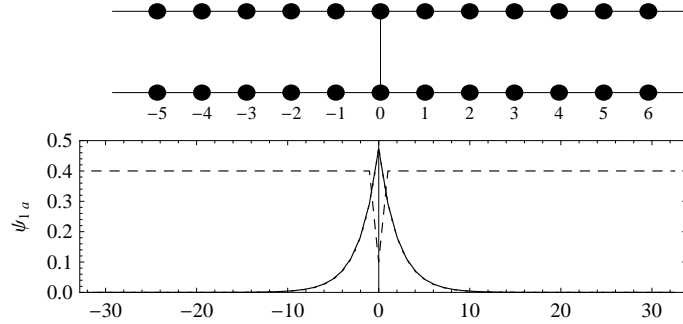

Fig. 10. Top: A ladder with a single rung at $a = 0$. Bottom: Plot of the numerically obtained ground-state wavefunction ψ_{1a} for $N = 32$ (solid line) compared with (6.12) (dotted line, hardly visible). The impurity potential V_a is also shown (dashed line, rescaled).

This is indeed what happens. Setting $E_1 = 3 - 2\cosh\theta$, *i.e.*, $\lambda_1 = 2\cosh\theta$, the (unnormalized) wavefunction reads

$$\psi_{1a} = \cosh((N - |a|)\theta). \tag{6.10}$$

The matching condition on the impurity yields the quantization condition

$$2\sinh\theta\,\tanh(N\theta) = 1. \tag{6.11}$$

The ground state is the unique bound state, corresponding to the real solution θ_1 to the latter equation. In the situation of most interest, namely N large, we obtain a non-trivial limiting solution so that $\sinh\theta_1 = 1/2$, $i.e.$, $\theta_1 = \ln((\sqrt{5}+1)/2)$, and hence $\lambda_1 = \sqrt{5}$. The limiting normalized ground-state wavefunction reads

$$\psi_{1a} = \frac{e^{-|a|\theta_1}}{\sqrt{\tanh\theta_1}}. \tag{6.12}$$

The particle performing MERW is localized in the vicinity of the attractive defect (rung). The stationary probability $\pi_a = \psi_{1a}^2$ of finding the particle at a distance a from the defect falls off exponentially as $\exp(-2|a|\theta_1)$. The corresponding localization length is $\xi = 1/\theta_1 = 2.078087$.

The existence of a localized ground state implies that the effective degree $K_3 = \lambda_1 = \sqrt{5} = 2.236068$ remains strictly larger than $K_1 = K_2 = 2$, even in the limit of an infinitely long system.

6.4. Diluted ladders

We now consider the disordered situation where impurities are distributed at random all over the ladder with some concentration q. In other words, we consider a diluted ladder graph where rungs are removed, independently of each other, with probability q. The tight-binding equation for the ground state is given by (6.1), where the potential V_a is a sequence of i.i.d. variables with the binary distribution

$$V_a = \begin{cases} 0 & \text{with probability } p, \\ 1 & \text{with probability } q = 1 - p. \end{cases} \tag{6.13}$$

The problem therefore maps onto the one-dimensional tight-binding Anderson model with diagonal disorder. Generic features of this model, such as the density of states or the localization length, have been investigated at length. In the present situation, we are however chiefly interested in the ground state of the model on a finite system of length L. This question is related to the behavior of the density of states $\rho(E)$ near the bottom of the spectrum ($E \to 0$). The latter is known to have the form of an exponentially small Lifshitz tail [25]. Lifshitz tails have been studied extensively, both from a mathematically rigorous standpoint [26] and in various physical contexts, including in particular the diffusion of particles in the presence of randomly placed absorbing traps [27].

In the one-dimensional case, the Lifshitz argument goes as follows. Low-lying states are expected to live on long wells, *i.e.*, ordered sequences of sites without impurities. Assume there is a well between sites b and c, *i.e.*, $V_b = V_c = 1$, whereas $V_a = 0$ for $b < a < c$. There will be an eigenstate living essentially on that well, and resembling the free mode on the well with Dirichlet boundary conditions at b and c, *i.e.*, $\psi_a \sim \sin((a-b)\pi/\ell)$, where $\ell = c - b$ is the length of the well. The corresponding energy is $E \approx \pi^2/\ell^2$. This line of thought can be used to estimate the fall-off of the density of states near the bottom of the spectrum ($E \to 0$). Long wells ($\ell \gg 1$) occur in the chain with an exponentially small probability of order p^ℓ. Eliminating ℓ for the corresponding energy E, we thus obtain

$$\rho(E) \sim \exp\left(-\frac{\pi |\ln p|}{\sqrt{E}}\right). \tag{6.14}$$

In the one-dimensional situation the above result is virtually exact, up to absolute prefactors involving oscillating functions [28]. The same picture can be used to estimate the ground-state energy E_1 on a finite system. According to a well-known argument of extreme-value statistics, the typical length ℓ_1 of the longest well on a finite system of length L is such that p^{ℓ_1} is of order $1/L$. We therefore predict that the ground state is typically localized in a Lifshitz well of length

$$\ell_1 \approx \frac{\ln L}{|\ln p|}, \tag{6.15}$$

and that the corresponding energy reads

$$E_1 \approx \left(\frac{\pi |\ln p|}{\ln L}\right)^2. \tag{6.16}$$

Figures 11 and 12 show linear and logarithmic plots of the stationary distribution of MERW on disordered ladders, obtained by a numerical diagonalization of the adjacency matrix for a system size $L = 512$. For $q = 0.01$ (see Figure 11), the estimate (6.15) yields $\ell \approx 620$. Both length scales L and ℓ are comparable, in agreement with the data showing a macroscopically large "dome". For $q = 0.1$ (see Figure 12), we obtain $\ell \approx 59$. Disorder is strong enough to observe the Lifshitz phenomenon, *i.e.*, the localization of the stationary distribution in the longest region without defects, which extends approximately between the positions -80 and -30, so that its length is indeed of order 50. The usual localization effect, *i.e.*, the exponential fall-off of the wavefunction over a characteristic length given by the localization length ξ, is also clearly visible on the lower panel of Figure 12.
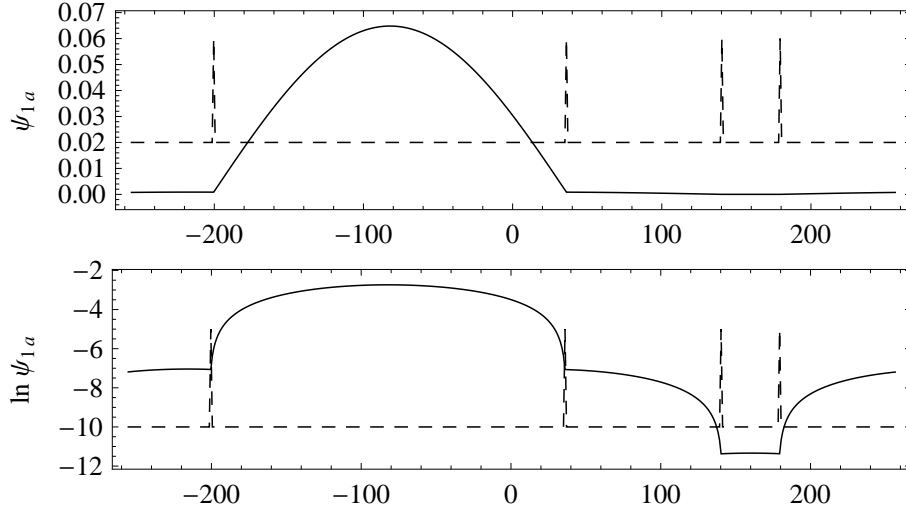
Fig. 11. Top: stationary distribution π_a of MERW on one configuration of the disordered ladder for a size $L = 512$ and a density $q = 0.01$ of defects. Bottom: same data plotted on a logarithmic scale. The impurity potential V_a is also shown (dashed line, rescaled).
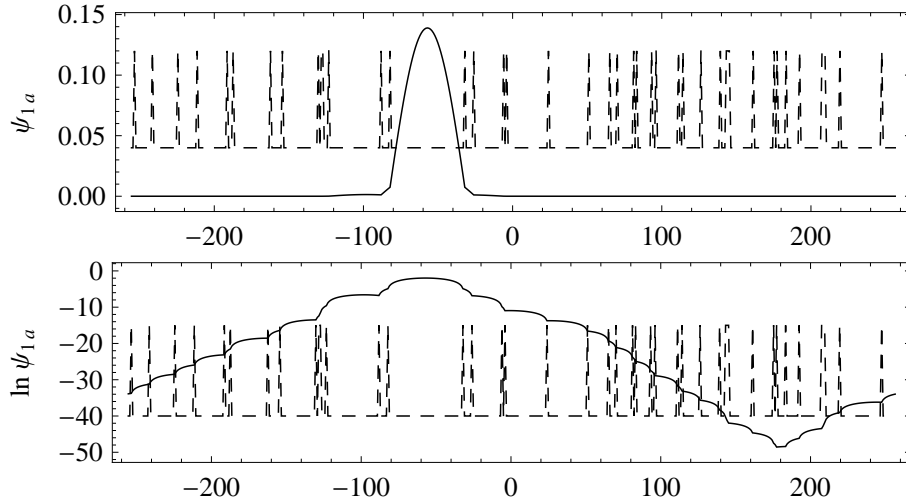

Fig. 12. Same as Figure 11, for a density of defects $q = 0.1$.

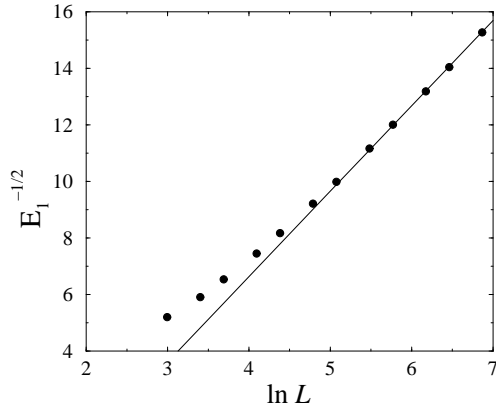Figure 13 shows a plot of $E_1^{-1/2}$ against $\ln L$, for a concentration of defects $q = 0.1$, and system sizes L ranging from 20 to 960. The ground-

Fig. 13. Plot of the inverse square root of the mean ground-state energy on disordered ladders against $\ln L$, for sizes $L = 20, \ldots, 960$ and $q = 0.1$. The solid line with slope $1/(\pi\,|\ln 0.9|)$ and a fitted intercept corroborates the estimate (6.16).

state energy has been obtained by diagonalizing numerically the adjacency matrix, and averaging the outcome over many disorder configurations. The data fully confirm the Lifshitz prediction (6.16). Finally, let us mention that the effective degrees $K_1 = 3 - q$ and $K_2 \approx 3 - 2q \ln(3/2) \approx 3 - 0.810930\,q$ depart linearly from the value 3 for an infinite ladder with a weak concentration q of defects, whereas $K_3 = 3 - E_1$ still goes asymptotically to 3, albeit with a logarithmic finite-size correction (see (6.16)).

6.5. The Fibonacci ladder

We close this section on ladders by considering a deterministic but non-periodic configuration of the removed rungs. We choose for definiteness the Fibonacci sequence $0100101001001010010100101001001\ldots$ This infinite sequence can be built in two alternative ways: either recursively, or by an explicit formula [29]. In the first method, the sequence is built as the fixed point of the substitution:

$$\sigma : \begin{cases} 0 \to 01 \\ 1 \to 0 \end{cases}, \tag{6.17}$$

acting on the two symbols 0 and 1, taking the symbol 0 as a seed. More explicitly, the recursion is initiated with a sequence of length one having only one symbol 0. Then, while moving along the sequence from left to right, one substitutes 0 by 01 and 1 by 0 until the last digit is reached. One then repeats the same procedure *ad infinitum*, thus generating the infinite Fibonacci sequence. The first steps of the recursion yield the words 0, 01,

010, 01001, 01001010, ... The lengths of these finite sequences are given by the consecutive Fibonacci numbers: 1, 2, 3, 5, 8, 13, ... Alternatively, the n-th symbol of the Fibonacci sequence is given by the explicit formula

$$V_n = \begin{cases} 1 & \text{if} \quad 0 < \text{Frac}(n\tau) < \tau^{-2}, \\ 0 & \text{if} \quad \tau^{-2} < \text{Frac}(n\tau) < 1, \end{cases} \tag{6.18}$$

where $\text{Frac}(x) = x - \text{Int}(x)$ denotes the fractional part of x, and

$$\tau = \frac{\sqrt{5}+1}{2} = 1.618033 \tag{6.19}$$

is the golden mean, such that $\tau^2 = \tau + 1$. The Fibonacci sequence is therefore both self-similar and quasiperiodic. It has become popular in the physics literature because it is a one-dimensional analogue of quasicrystals, discovered in 1984 [30]. The density of zeros, *i.e.*, rungs, and ones, *i.e.*, impurities, along the infinite Fibonacci ladder read $p = \tau^{-1} = \tau - 1 = 0.618033$ and $q = \tau^{-2} = 2 - \tau = 0.381966$, respectively.

We have considered finite Fibonacci ladders of variable length N (not necessarily even), with periodic boundary conditions, where the positions of the rungs is dictated by the impurity potentials V_n from Eq. (6.18) for $n = 1, \ldots, N$. A numerical diagonalization of the corresponding adjacency matrices leads to the following observations. The largest eigenvalue λ_1 keeps oscillating as a function of the ladder size N between the asymptotic bounds $\lambda_{\min} \approx 2.6945$ and $\lambda_{\max} \approx 2.7472$. These oscillations appear as regular if λ_1 is plotted against the phase $\text{Frac}((N+1)\tau)$ (see Figure 14). The modulation of the largest eigenvalue λ_1 as a function of N therefore follows the quasiperiodicity of the underlying sequence.

The ground state (Perron-Frobenius eigenvector) ψ_{1n} also exhibits irregular features. Its appearance varies from localized to extended as a function of the system size N. Figure 15 shows one typical example of each kind. As a general rule, the ground state looks pretty localized when λ_1 is close to $\lambda_{\max}$, *i.e.*, when $\text{Frac}((N+1)\tau)$ is close to zero. This is illustrated by the left panel of the figure, where $N = 232$ and $\lambda_1 = 2.747147 \approx \lambda_{\max}$: the ground state appears as a symmetric impurity state localized at the boundary, *i.e.*, around $n = 0$. On the other hand, the ground state looks pretty extended when λ_1 is close to $\lambda_{\min}$, *i.e.*, when $\text{Frac}((N+1)\tau)$ is far from zero. This is illustrated by the right panel, where $N = 377$ and $\lambda_1 = 2.694529 \approx \lambda_{\min}$: the ground state exhibits quite some structure, but it extends more or less uniformly over the whole ladder. Let us however recall that the tight-binding Hamiltonian (6.1) on the Fibonacci chain is known from a rigorous viewpoint to have a purely singular continuous spectral measure, so that its eigenstates are neither extended nor localized (see [31] for a review). Generic eigenstates are observed to be multifractal.
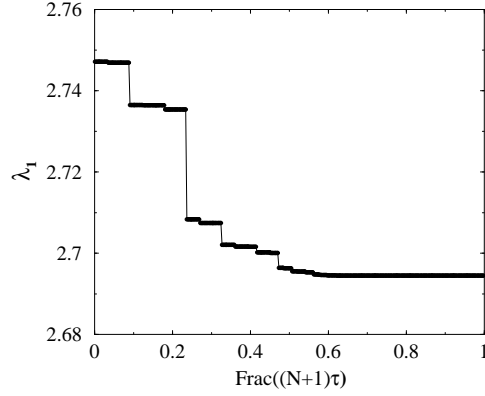
Fig. 14. Plot of the largest eigenvalue λ_1 of the Fibonacci ladder of size N against the phase $\text{Frac}((N + 1)\tau)$.
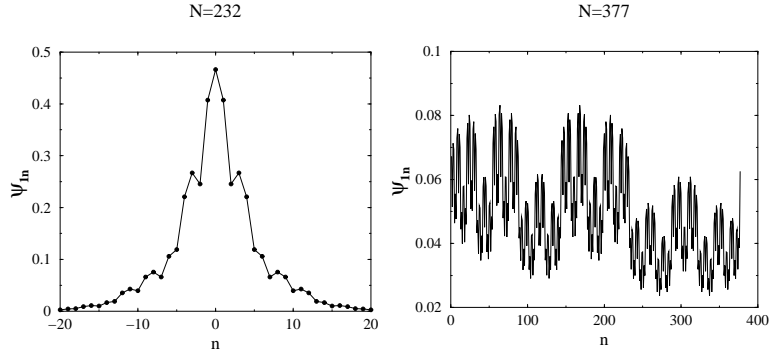

Fig. 15. Plot of the ground-state wavefunction ψ_{1n} in two typical examples of finite Fibonacci ladders. Left: $N = 232$, $\lambda_1 = 2.747147$. Right: $N = 377$, $\lambda_1 = 2.694529$.

7. Two-dimensional examples

In this last section, we pursue our study of MERW on extended structures by considering a few two-dimensional situations of interest.

7.1. Diffusion on the dual $(4, 8^2)$ lattice

We start by an investigation of the transport properties associated with GRW and MERW on infinite periodic lattices. The simplest non-trivial two-dimensional example of a non-bipartite periodic lattice is shown in Figure 16. This lattice is dual to the $(4, 8^2)$ Archimedean lattice [32, 33]. Nodes denoted by "●" with degree $k_\bullet = 8$ and nodes denoted by "○" with degree

$k_\circ = 4$ have equal densities. It can be checked that $\lambda_1 = 2(\sqrt{5}+1)$, whereas $\psi_{1\bullet} : \psi_{1\circ} = (\sqrt{5}+1)/2$. The effective degrees of the infinite lattice thus read

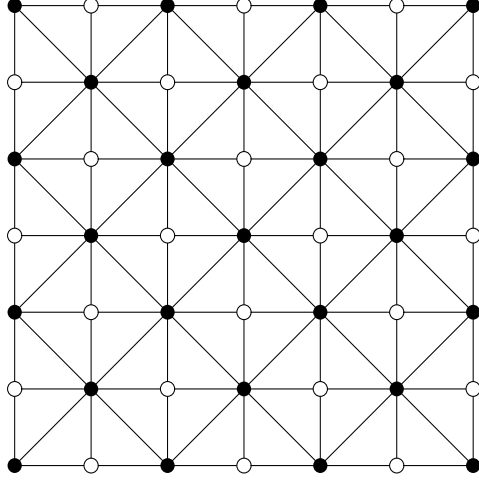$$K_1 = 6, \qquad K_2 = 2^{8/3} = 6.349604, \qquad K_3 = 2(\sqrt{5}+1) = 6.472135. \quad (7.1)$$

Fig. 16. A finite sample of the dual $(4, 8^2)$ lattice.

Both GRW and MERW can be viewed as two special cases of the one-parameter family of discrete-time random walks defined by the following hopping probabilities onto neighboring nodes:

$$P_{\bullet\bullet} = \frac{1+\alpha}{8}, \qquad P_{\circ\bullet} = \frac{1-\alpha}{8}, \qquad P_{\bullet\circ} = \frac{1}{4}, \qquad (7.2)$$

where the parameter α is in the range $-1 \leq \alpha \leq 1$. GRW and MERW can be shown to correspond to $\alpha = 0$ and $\alpha = \sqrt{5} - 2 = 0.236068$, respectively.

In order to investigate transport properties, it is advantageous to rewrite the master equation (3.1) in Fourier space. Denoting by x and y the coordinates on the lattice, we set

$$p_\bullet(x,y,\tau) = \int \frac{\mathrm{d}u\,\mathrm{d}v}{(2\pi)^2}\, \widehat{p}_\bullet(u,v,\tau)\,\mathrm{e}^{-\mathrm{i}(xu+yv)}, \qquad (7.3)$$

and similarly for $p_\circ(x,y,\tau)$, where u and v are the components of the wavevector, and the integral runs over the first Brillouin zone ($-\pi < u, v < \pi$). From Eq. (3.1) we obtain

$$\begin{pmatrix} \widehat{p}_\bullet(u,v,\tau+1) \\ \widehat{p}_\circ(u,v,\tau+1) \end{pmatrix} = \Omega(u,v) \begin{pmatrix} \widehat{p}_\bullet(u,v,\tau) \\ \widehat{p}_\circ(u,v,\tau) \end{pmatrix}, \qquad (7.4)$$

with

$$\Omega(u, v) = \begin{pmatrix} 4P_{\bullet\bullet} \cos u \cos v & 2P_{\bullet\circ}(\cos u + \cos v) \\ 2P_{\circ\bullet}(\cos u + \cos v) & 0 \end{pmatrix}. \qquad (7.5)$$

In the long-wavelength limit, *i.e.*, for small u, v, the largest eigenvalue of this dynamical matrix departs from unity according to

$$\omega(u, v) \approx 1 - \frac{u^2 + v^2}{3 - \alpha} + \cdots \qquad (7.6)$$

This behavior demonstrates that isotropic diffusion is recovered for all values of α. The corresponding diffusion constant,

$$D(\alpha) = \frac{1}{3 - \alpha}, \qquad (7.7)$$

increases as a function of α from $1/4$ to $1/2$. Its values for GRW and MERW read

$$D_{\mathrm{GRW}} = \frac{1}{3} = 0.333333, \qquad D_{\mathrm{MERW}} = \frac{5 + \sqrt{5}}{20} = 0.361803. \qquad (7.8)$$

This example shows that MERW can lead to a higher diffusion constant, *i.e.*, better transport properties, than GRW on some periodic lattices.

7.2. Designed patterns

In order to investigate the effect of impurities on MERW in higher dimensions, before going to the disordered situation of a diluted lattice, we find it interesting to first look at MERW on designed patterns consisting of simple geometrical shapes drawn on purpose.

Figure 17 shows two examples of patterns drawn on a square lattice with periodic boundary conditions. The fully connected square lattice is left untouched in some regions, so as to have the maximal degree 4, and hence no repulsive potential, whereas every second horizontal bond is removed in some other regions, so as to have degree 3, and hence a constant repulsive potential of unit magnitude. Consider first the left panel of Figure 17. The fully connected regions are four circles of various sizes. The stationary distribution π_a, evaluated by numerically diagonalizing the adjacency matrix, is shown as levels of gray. It is clearly visible that the stationary MERW distribution gets localized in the largest circle. Another numerical experiment is shown in the right panel of Figure 17. This time we have four different shapes, all of them having the same area. The stationary distribution is observed to localize in the circular region. To sum up, given a set of domains without defects (where nodes have the highest degree), a particle performing MERW tends to spend most of its time, and gets eventually localized, in the largest and most circular of these domains.
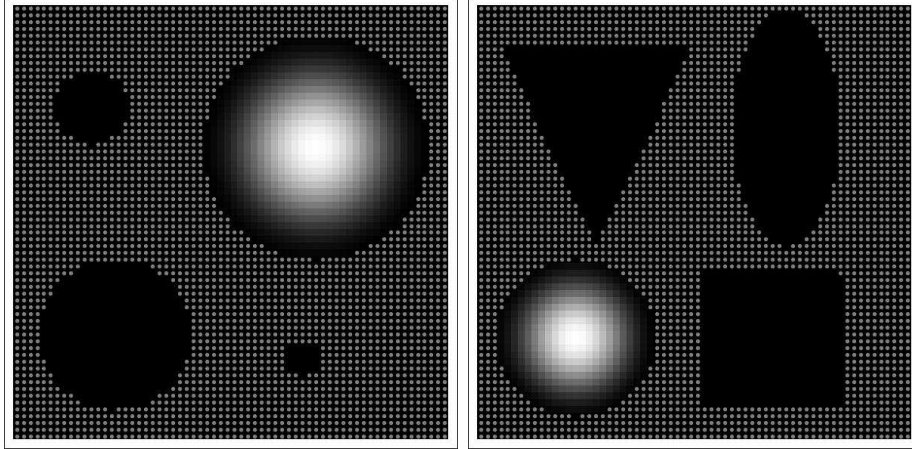
Fig. 17. Two examples of designed patterns drawn on a square lattice with periodic boundary conditions. Textured regions have a constant unit repulsive potential. The stationary distribution of MERW is shown as levels of gray (white: highest probability, black: zero probability).

7.3. The diluted square lattice: stationary state

We now turn to the case of the diluted square lattice, where bonds are removed at random with a (small) probability q.

The Lifshitz argument presented in Section 6.4 generalizes to higher dimensions [26, 27]. The ground state is expected to be localized in the largest *Lifshitz region*, *i.e.*, nearly circular region free of defects. The quantitative analysis of the phenomenon goes as follows. The radius R_1 of the largest Lifshitz region can be estimated by means of extreme-value statistics. On a finite system of size $L \times L$, the number of nearly circular regions of radius R with no defect is of order $L^2 p^{2\pi R^2}$, as there are two links per node. The criterion that this number becomes of order unity yields

$$R_1 \approx \left(\frac{\ln L}{\pi \, |\ln p|} \right)^{1/2} . \tag{7.9}$$

Now, using a continuum description, the ground state in the disk of radius R_1 with Dirichlet boundary conditions is given by $\psi(r) \sim J_0(jr/R_1)$, where r is the distance from the center, and $j = 2.404825\ldots$ is the first zero of the Bessel function J_0. We thus obtain

$$E_1 \approx \left(\frac{j}{R_1} \right)^2 \approx \frac{\pi j^2 \, |\ln p|}{\ln L} . \tag{7.10}$$

The corresponding thermodynamical statement, generalizing (6.14), reads

$$\rho(E) \sim \exp\left(-\frac{2\pi j^2 \,|\ln p|}{E}\right).$$ (7.11)

This picture is corroborated by the data shown in Figure 18. The stationary probability, shown as levels of gray, is observed to be localized in the largest nearly circular regions free of defects. Their sizes are in rough agreement with the estimate (7.9), yielding, respectively, $R_1 = 34.3$, 10.8, 4.78 and 3.34 for $q = 0.001$, 0.01, 0.05 and 0.1.
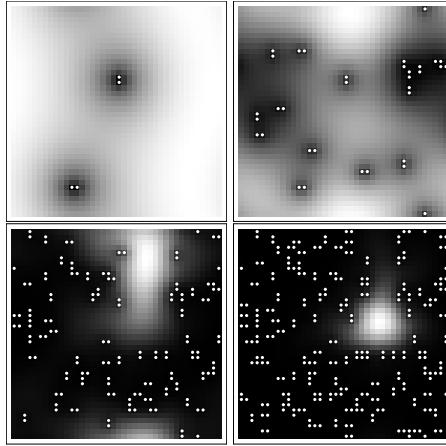

Fig. 18. Density plots of the stationary distribution for MERW on a 40×40 square lattice with periodic boundary conditions, for the concentrations $q = 0.001, 0.01, 0.05, 0.1$ of removed links. The endpoints of removed links are shown as bright dots. The stationary probability is shown as levels of gray.

In higher dimension $(d \geq 2)$, skipping lattice-dependent multiplicative constants, the above estimates become

$$-\ln \rho(E) \sim \frac{|\ln p|}{E^{d/2}},$$ (7.12)

and

$$R_1 \sim \left(\frac{\ln L}{|\ln p|}\right)^{1/d}, \qquad E_1 \sim \left(\frac{|\ln p|}{\ln L}\right)^{2/d},$$ (7.13)

where L is the linear size of the sample. Hence the stationary distribution of MERW on a sufficiently large d-dimensional lattice in the presence of any finite concentration q of disorder is localized in the largest nearly spherical Lifshitz region whose volume grows as $\ln L$.

Let us close up with a word on the weak-disorder crossover. When the amount of disorder gets smaller and smaller ($q \ll 1$), the volume of the Lifshitz sphere diverges as $\Omega_1 \sim R_1^d \sim (\ln L)/q$. When this estimate is of the order of the volume L^d of the sample, MERW experiences a crossover between a Lifshitz localized regime (for $L^d \gg \Omega_1$, *i.e.*, $qL^d \gg \ln L$) and an extended regime (for $L^d \ll \Omega_1$, *i.e.*, $qL^d \ll \ln L$). The number qL^d of impurities needed to drive the crossover is therefore very modest, as it also grows as $\ln L$.

7.4. The diluted square lattice: dynamics

So far, we have seen that the stationary distributions for GRW and MERW are qualitatively different in the presence of disorder, such as a weak dilution. A particle performing MERW will eventually end up in the largest Lifshitz sphere, *i.e.*, the largest nearly spherical region free of defects, where the stationary distribution is localized. Inside this region, MERW will look much like usual random walk, *i.e.*, like Brownian motion on large space and time scales.

In the transient regime, *i.e.*, before the particle finds its stationary state, it is expected to stay for a while in some Lifshitz region, smaller than the optimal one but nearer to its starting point, where it will spend some time, before it "learns" that there is a better, albeit more distant, region elsewhere in the system, and so on. The diffusion process will thus explore a sequence of consecutive metastable states, depending on the initial point, before finally reaching the true ground state. A similar picture should hold for a diffusive particle in the presence of a random distribution of absorbing traps [27], if the observation is conditioned on the survival of the particle. We can therefore expect the dynamics to exhibit two different time scales, just as in many glassy systems (see *e.g.* [34]): a fast *(beta)* relaxation within each metastable Lifshitz region (where the entropy can be maximized locally), and a slow *(alpha)* relaxation corresponding to tunneling between consecutive Lifshitz regions, until the optimal region which carries the true ground state is reached, so that the entropy production rate has attained its maximal value.

This difference between the dynamical evolution of GRW and MERW is illustrated in Figure 19. A particle performing GRW (upper panels) and MERW (lower panels) starts at the same site of a lattice with the same randomly positioned defects. In the course of evolution, the generic random walker visits every site with a probability proportional to its degree. After a sufficiently long time, the probability distribution spreads more or less uniformly over the lattice. The stationary distribution is locally modulated by the presence of impurities, but it remains globally extended, just as in
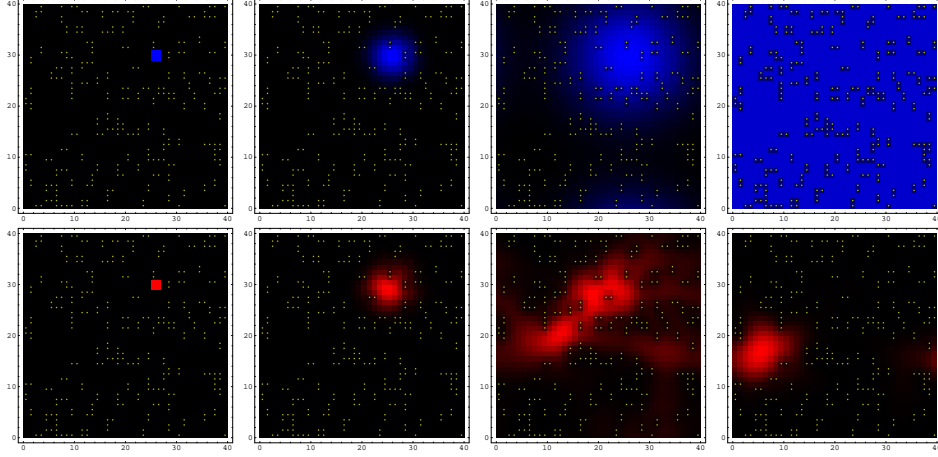
Fig. 19. (Color online). Evolution of GRW (upper panels) and MERW (lower panels) on a 40×40 square lattice with a concentration $q = 0.1$ of removed links. Left to right: distribution after 1, 16, 128 time steps and in the stationary state.

the case of a lattice without defects. The situation for the maximal entropy random walker is quite different. The particle indeed visits a sequence of larger and larger, albeit more and more distant regions free of defects, until it eventually reaches its stationary state.

Acknowledgments

REFERENCES

[1] A. Einstein, Ann. Physik **17**, 547 (1905); **19**, 371 (1906).

[2] M. Smoluchowski, Ann. Physik **21**, 756 (1906).

[3] B.D. Hughes, *Random Walks and Random Environments. Volume 1: Random Walks* (Oxford University Press, Oxford, 1995).

[4] W. Feller, *An Introduction to Probability Theory and its Applications*, in 2 volumes (Wiley & Sons, New-York, 1966).

[5] E.W. Montroll and B.J. West, in *Studies in Statistical Mechanics VII: Fluctuation Phenomena*, edited by E.W. Montroll and J.L. Lebowitz (North-Holland, Amsterdam, 1979).

[6] R.P. Feynman and A.R. Hibbs, *Quantum Mechanics and Path Integrals* (Mc Graw-Hill, New York, 1965).

[7] Z. Burda, J. Duda, J.M. Luck, and B. Waclaw, Phys. Rev. Lett. **102**, 160602 (2009).

[8] B. Waclaw, *Generic Random Walk and Maximal Entropy Random Walk*, from The Wolfram Demonstrations Project, http://demonstrations.wolfram.com/GenericRandomWalkAndMaximalEntropyRandomWalk/

[9] R.J. Wilson, *Introduction to Graph Theory*, 2nd ed. (Longman, London, 1979).

[10] B. Bollobas, *Modern Graph Theory* (Springer, New York, 1998).

[11] J. Gómez-Gardeñes and V. Latora, Phys. Rev. E **78**, 065102(R) (2008).

[12] R. Bellman, *Introduction to Matrix Analysis* (McGraw-Hill, New York, 1970); H. Minc, *Nonnegative Matrices*, Series in Discrete Mathematics and Optimization (Wiley, New York, 1986); R.B. Bapat and T.E.S. Raghavan, *Nonnegative Matrices and Applications*, Encyclopedia of Mathematics and Its Applications, vol. 64 (Cambridge University Press, Cambridge, 1996).

[13] C. Itzykson and J.M. Drouffe, *Statistical Field Theory*, in 2 volumes (Cambridge University Press, Cambridge, 1989).

[14] J. Ambjørn, Z. Burda, J. Jurkiewicz, and C.F. Kristjansen, Acta Phys. Pol. B **23**, 991 (1992).

[15] H. Kawai, N. Kawamoto, T. Mogami, and Y. Watabiki, Phys. Lett. B **306**, 19 (1993); Y. Watabiki, Nucl. Phys. B **441**, 119 (1995); J. Ambjørn and Y. Watabiki, Nucl. Phys. B **445**, 129 (1995); F. David, Nucl. Phys. B **257**, 45 (1985); J. Ambjørn, B. Durhuus, and J. Fröhlich, Nucl. Phys. B **257**, 433 (1985); V.A. Kazakov, I.K. Kostov, and A.A. Migdal, Phys. Lett. B **157**, 295 (1985).

[16] J. Ambjørn and R. Loll, Nucl. Phys. B **536**, 407 (1998); J. Ambjørn, J. Nielsen, J. Rolf, and R. Loll, Chaos Solitons Fractals **10**, 177 (1999); J. Ambjørn, J. Jurkiewicz, and R. Loll, Phys. Rev. Lett. **95**, 171301 (2005).

[17] J. Zinn-Justin, *Quantum Field Theory and Critical Phenomena* (Clarendon, Oxford, 1989).

[18] R. Albert and A.L. Barabási, Rev. Mod. Phys. **74**, 47 (2002); S.N. Dorogovtsev and J.F.F. Mendes, *Evolution of Networks* (Oxford University Press, Oxford, 2003); S. Boccaletti, V. Latora, Y. Moreno, M. Chavez, and D.U. Hwang, Phys. Rep. **424**, 175 (2006); A. Barrat, M. Barthélemy, and A. Vespignani, *Dynamical Processes on Complex Networks* (Cambridge University Press, Cambridge, 2008).

[19] J.G. Kemeny and J.L. Snell, *Finite Markov Chains* (Van Nostrand, Princeton, 1960).

[20] C. Shannon, Bell System Tech. J. **27**, 379 (1948); C. Shannon and W. Weaver, *The Mathematical Theory of Communication* (University of Illinois Press, Urbana, 1949).

[21] W. Parry, Trans. Amer. Math. Soc. **112**, 55 (1964).

[22] M. Brin and G. Stuck, *Introduction to Dynamical Systems* (Cambridge University Press, Cambridge, 2002).

[23] J.H. Hetherington, Phys. Rev. A **30**, 2713 (1984).

[24] N. O'Connell, J. Phys. A **36**, 3049 (2003).

[25] I.M. Lifshitz, Adv. Phys. **13**, 483 (1964); Sov. Phys. – Uspekhi **7**, 549 (1965).

[26] L. Pastur, Russ. Math. Surv. **28**, 1 (1973); R. Friedberg and J.M. Luttinger, Phys. Rev. B **12**, 4460 (1975); S. Nakao, Jpn. J. Math. **3**, 111 (1977); W. Kirsch and F. Martinelli, Commun. Math. Phys. **89**, 27 (1983).

[27] B.Y. Balagurov and V.G. Vaks, Sov. Phys. – J.E.T.P. **38**, 968 (1974); M.D. Donsker and S.R.S. Varadhan, Commun. Pure Appl. Math. **28**, 525 (1975); **32**, 721 (1979); P. Grassberger and I. Procaccia, J. Chem. Phys. **77**, 6281 (1982); J.W. Haus and K.W. Kehr, Phys. Rep. **150**, 263 (1987); Th.M. Nieuwenhuizen, Phys. Rev. Lett. **62**, 357 (1989); Physica A **167**, 43 (1990).

[28] Th.M. Nieuwenhuizen and J.M. Luck, Physica **145A**, 161 (1987); J. Stat. Phys. **48**, 393 (1987); J.M. Luck, *Systèmes Désordonnés Unidimensionnels* (In French) (Collection Aléa-Saclay, 1992).

[29] R.L. Graham, D.E. Knuth, and O. Patashnik, *Concrete Mathematics: a Foundation for Computer Science* (Addison-Wesley, Reading, Mass., 1989).

[30] D. Shechtman, I. Blech, D. Gratias, and J.W. Cahn, Phys. Rev. Lett. **53**, 1951 (1984).

[31] D. Damanik, in *Directions in Mathematical Quasicrystals*, M. Baake and R.V. Moody (Eds.), CRM Monograph Series (Amer. Math. Soc., Providence, 2000).

[32] J. Kepler, *Harmonices Mundi* (Lincii, 1619).

[33] B. Grünbaum and G.C. Shephard, *Tilings and Patterns* (Freeman, New York, 1987).

[34] J.L. Barrat et al. (Eds.), *Slow Relaxations and Nonequilibrium Dynamics in Condensed Matter* (Les Houches Session LXXVII, 1-26 July, 2002) (Springer, New York, 2003).